The contribution of large scale structures in the power generation of finite scale wind farms using large eddy simulation

Tanmoy Chatterjee

Mechanical and Aerospace Engineering
School of Matter Transport and Energy,
Arizona State University
501 E. Tyler Mall, Tempe, AZ 85287
email: tchatte3@asu.edu

Yulia Peet

Mechanical and Aerospace Engineering
School of Matter Transport and Energy,
Arizona State University
501 E. Tyler Mall, Tempe, AZ 85287
email: ypeet@asu.edu

ABSTRACT

The large scale organizations in the flow around the finite scale wind farms that contribute to the turbine power, have been studied in the current paper. The study has been carried out using Large Eddy Simulation (LES) with near wall modelling, and the turbine forces are modelled using the actuator line model. Proper orthogonal decomposition (POD) has been used as a tool of analysis to understand the large scale features contributing to the power generation by wind turbines in different rows of a wind farm. The POD modes reveal the existence of energetic flow features significantly larger than the turbine rotor diameter contributing to the flux of the mean kinetic energy (MKE). Thes fluxes play an instrumental role in power generation as also observed in the previous literature. New insights on the flow structures around the wind farm have been obtained which opens up further research directions to understand the localized transfer of the MKE flux.

INTRODUCTION

Large wind farms in atmospheric boundary layer (ABL) are often studied in the asymptotic limit of infinite number of wind turbine rows, where the flow past the wind turbines is fully developed given by periodic boundary conditions in the streamwis and spanwise directions as seen in Frandsen *et al.* (2006), Calaf *et al.* (2010), and describable through simple equilibrium laws. This assumption essentially neglects many complex flow features like the growth of the inner layer due to the turbulent dispersion of the wakes, impingement of the wakes from one row of wind turbines to the next row and beyond, which typically results in a decreased power and an increased structural loading of the downstream turbines. More importantly, these flow features which arise due to the spatial variability of the convection of kinetic energy, cannot be neglected for wind farms where the streamwise and spanwise extent of the layout are comparable to the atmospheric boundary layer thickness.

The previous literature has shown the contribution of large scale structures responsible for the power generation in infinite wind farms, e.g., using Fourier analysis by Chatterjee & Peet (2016*b*) and proper orthogonal decomposition (POD) by VerHulst & Meneveau (2014). Hamilton *et al.* (2016) looked at proper orthogonal decomposition of an experimental database, but they also focused on a homogeneous part of the wind farm beyond the fourth row, that can be approximated by the fully developed condition and row-to-row periodicity. To the authors knowledge, no such study has been performed to understand the behaviour of large scale features in the power generation of aperiodic, finite scale wind farms. Understanding the multi scale dynamics involved in the interaction of large scale atmospheric flows with the wind turbine rotors in the first and subsequent rows is important, as this will improve our interpretation of power generation in wind turbine arrays required for an efficient optimization of the wind farm layout. For infinite wind farms with homogeneity in the horizontal direction, Fourier analysis is a natural choice for studying the length scales of motion. However, in finite scale wind farms, the streamwise inhomogeneity due to the inner layer growth, renders the use of Fourier analysis to be limited. Consequently, in the current paper, we propose to present the POD analysis of the flow features past the wind turbine array, and also to understand the variation of large scale modal structures that contribute to the power compared to infinite wind farms.

NUMERICAL METHOD

The numerical method implements a variational formulation of the Navier-Stokes equations involving Galerkin projection using an exponentially accurate open-source spectral element (SEM) solver **Nek5000** (See Fischer *et al.* (2008)). The numerical simulations at Reynolds number 10^{10} based on the hub-height velocity and the boundary layer thickness are carried out using Large Eddy Simulation (LES) with near wall modelling, and the wind turbine forces are modelled using the state-of-the-art actuator line model (Refer to Chatterjee & Peet (2016*a*,*b*) for details of the model). To provide a validation of our spectral element LES near-wall modeling methodology, we plot the non-dimensional streamwise velocity gradient and streamwise kinetic energy spectra for the LES simulations of a neutral ABL in Figure 1 that shows correct logarithmic trends of the streamwise velocity profile as well as the appropraite scaling laws of k_x^{-1} (overlap between inertial and integral scales) and $k_x^{-5/3}$ (overlap between inertial and dissipation scales) as measured by Perry *et al.* (1986).

The computational domain is rectangular and cartesian, of the size $3\pi H \times \pi H \times H$ in streamwise, spanwise and wall-normal directions, respectively, with H being the ABL thickness. The domain consists of a 3×3 organized array of wind turbines, with the rotor diameter $D = 0.2H$. The streamwise and spanwise inter-turbine distances are $7D$ and $3D$ respectively, with the first row of turbines placed πH distance from the inlet boundary. The spanwise boundary conditions are periodic, the top boundary condition is stress free and the bottom boundary has a shear-stress boundary condition corresponding to the near wall modelling of the log law of the wall (Chatterjee & Peet (2016*a*,*b*)). The inflow boundary condition is generated from a separate precursor simulation of a neutral periodic ABL flow with the domain size $2\pi H \times \pi H \times H$, while stabilized outflow boundary conditions have been used at the streamwise outlet of the wind turbine domain (Refer to Chatterjee & Peet (2016*a*) for details of inflow-outflow boundary condition). LES simulations of a flow past the 3×3 wind turbine array with the inflow-outflow boundary conditions were performed for the duration of 100 flow-through times to ensure statistical stationarity, after which snapshots and statistics were collected for 100 more flow through times for the POD analysis.

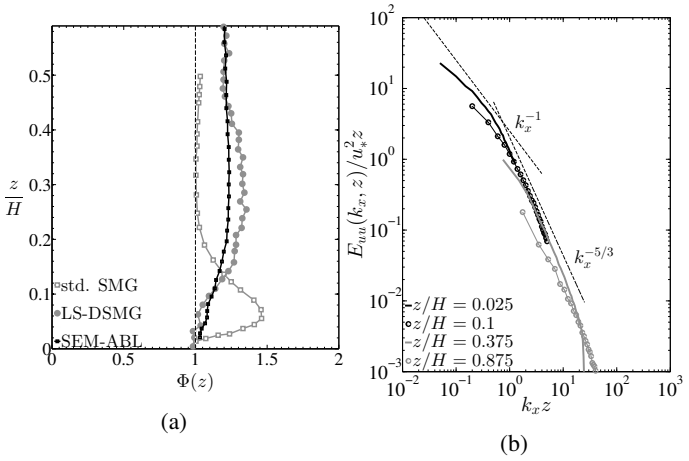

(a) (b)

Figure 1: (a) Non-dimensional streamwise velocity gradient $\Phi(z) = \kappa z/u_* d\overline{U}/dz$ vs z/H. Plots of standard wall-damped Smagorinsky (std. SMG) and Lagrangian Scale dependent dynamic Smagorinsky (LS-DSMG) model from Bou-Zeid *et al.* (2005). (b) Streamwise energy spectra $E_{uu}(k_x,z)/u_*^2 z$ at different locations from the wall., k_x – streamwise wavenumber, u_* – wall friction velocity. Results from the current SEM-ABL.

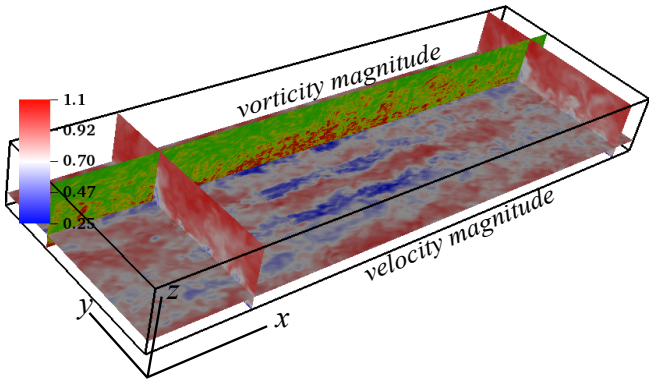

Figure 2: Temporal snapshot of normalized velocity magnitude $\sqrt{u^2+v^2+w^2}/U_\infty$ and vorticity magnitude $\sqrt{\omega_x^2+\omega_y^2+\omega_z^2}/U_\infty$ in a 3×3 wind turbine array. U_∞ is mean freestream velocity. Velocity: xy plane at hub-height $z_h = 0.2H$. yz plane at $x = \pi H$ (first row of turbines) and $x = 2.7\pi H$. Vorticity: xz plane at $y = \pi H/2 + 3D$ (last column of turbines), contour values -10 to 10.

TURBULENT STATISTICS AND SPECTRA

Figure 2 shows the normalized velocity and vorticity magnitude contours at different regions of the flow past the 3×3 turbine array. The contour plots of the mean and turbulent statistics can be found in Figure 3. The second order statistics such as turbulent kinetic energy, mean kinetic energy flux, turbulence production, manifest the growth of the inner layer and the wake-impingement effects, with increased "turbulent activity" in the second and third row of turbines.

The 1D streamwise energy spectra $E_{uu}(k_x,z)$ for the wind turbine array in Figure 4 indicates the presence of the robust k_x^{-1} law near the wall, even though, unlike in the periodic ABL case, the spectra does not collapse well with the normalized scaling of $u_*^2 z$.

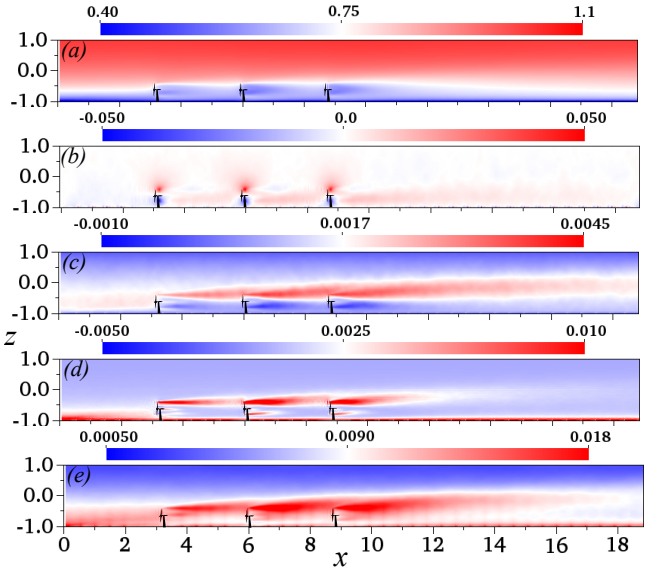

Figure 3: xz plane of temporally and spanwise averaged normalized mean and turbulent statistics. (a) streamwise velocity $\overline{U}$ (b) wall-normal velocity $\overline{W}$ (c) mean kinetic energy flux $-\overline{u_i' u_j'}\bar{U}_i$ (d) dominant term of turbulence production $-\overline{u'w'}\frac{\partial \bar{U}}{\partial z}$ (e) Turbulent kinetic energy $1/2\overline{u_i' u_i'}$. Normalization velocity U_∞, normalization distance H.

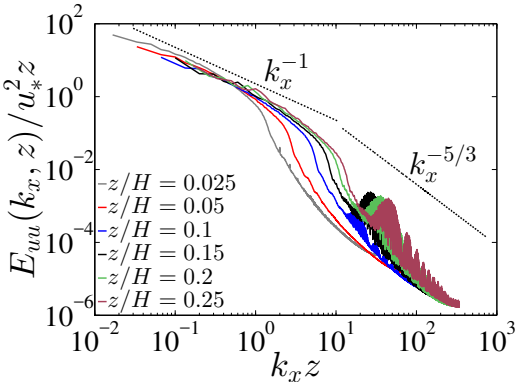

Figure 4: 1D normalized streamwise energy spectra $E_{uu}(k_x,z)/u_*^2 z$ in the wind turbine array. u_* – friction velocity of ABL, k_x – streamwise wave number.

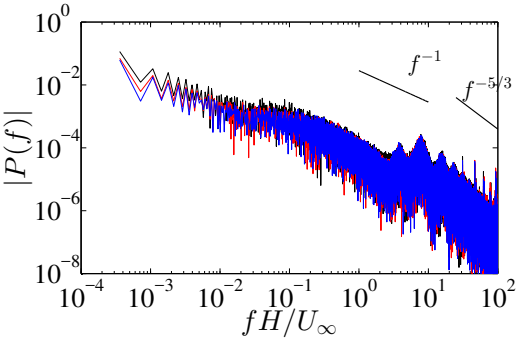

Figure 5: Power spectral density of the power of wind turbines averaged over the first row (black), second row (red) and third row (blue).

Since similar spectra in the periodic wind farms (Chatterjee & Peet (2016*b*)) also shows the lack of collapse, the streawise inner layer growth is unlikely the reason, which means that it is likely the hub-height dynamics of the wind turbines that is conspicuously different from a more familiar log-layer dynamics in the atmospheric boundary layer. The peaks in the spectra indicate length scales of eddies which are intercepted by the rotation of the wind turbine blades. It must be noted that the Fourier coefficients used in the spectra are obtained by using the continous Fourier integral, rather than a discrete Fourier transform, to account for streamwise aperiodicity. The power spectral density (PSD) of the wind turbine powers in Figure 5 also displays similar scaling and the peaks in the spectra, now in frequency domain, analogous to the spatial energy spectra as discussed above. The PSD further manifests that the differences in turbine power due to the wake impingements manifested in lower turbine power in the 2^{nd} and 3^{rd} row of turbines is also a low frequency-phenomenon corresponding to larger temporal scales of $O(\sim 10^3 H/U_\infty)$.

RESULTS AND DISCUSSION

POD: Method of Snapshots

The POD analysis was carried out using the *method of snapshots* by Sirovich (1987). In the discrete framework, the velocity vector field $u_i(\mathbf{x},t_n)$ $(i=1,2,3)$, as a function of space and time can be decomposed into a set of orthonormal basis functions,

$$u_i(\mathbf{x},t_n) = \overline{u}_i(\mathbf{x}) + \sum_{m=1}^{N} a_m(t_n)\phi_m^i(\mathbf{x}) \tag{1}$$

where $\overline{u}_i(\mathbf{x})$ is the time averaged velocity field and t_n, $\forall n = 1,\ldots,N$ is the discrete time in which the snapshots were collected. The orthonormal basis functions can be constructed from the velocity fields stored at some specific intervals of time (snapshots), such that the functions ϕ_m^i are maximized in the energy content, in a least squares sense. For example, with velocity snapshots at different times, $u_i(\mathbf{x},t_n)$, the basis functions can be reconstructed as a weighted sum of these snapshot quantities as shown in Equation 2.

$$\phi_m^i(\mathbf{x}) = \sum_{n=1}^{N} \frac{a_m(t_n)}{\lambda_m N}(u_i(\mathbf{x},t_n) - \overline{u}_i(\mathbf{x})) \tag{2}$$

The solution to this optimization problem essentially leads to an eigenvalue problem, where $\phi_m^i(\mathbf{x})$ are the u, v, w velocity based eigenfunctions corresponding to $i=1,2,3$, and the basis functions satisfy $(\phi_k^i(\mathbf{x}),\phi_l^i(\mathbf{x}))_\Omega = \delta_{kl}$, with the orthormality obtained from the inner product taken over the whole domain Ω. The eigenvalue λ_m represents the energy content of the m^{th} mode. The eigenvectors are $e_m(t_n) = a_m(t_n)/\sqrt{\lambda_m N}$ obtained from the POD matrix eigenvalue problem (See Sirovich (1987); Berkooz *et al.* (1993), for details of the derivation). The POD eigenvalue solver in spectral elements has been developed native to Nek5000 and has been validated with the 2D flow past a cylinder from Merzari *et al.* (2011). In the current study the sampling frequency of the snapshots is taken to be $\sim 2.5H/U_\infty$, which is equivalent to roughly $\sim 10D/U_{hub}$, where U_{hub} is the hub-height velocity, i.e. ten times the time scale of eddies intercepted by wind turbine blades. From Equation 2, it is apparent, that all the characteristics of the snapshot velocities, e.g., divergence free constraint, spanwise periodicity are also present in the orthonormal eigenfunctions $\phi_m^i(\mathbf{x})$.

Figure 6 shows a snapshot of kinetic energy of fluctuations of the flow past the wind turbine array indicating the existence of fluctuation kinetic energy $\frac{1}{2}u_i'u_i'$ as large as $\sim 10\%$ of the free-stream kinetic energy $\frac{1}{2}U_\infty^2$ around the wind turbine rotors. The POD modes discussed in the subsequent paragraphs aim at identifying the energetic structures contained in a cumulative distribution of such snapshots (Figure 6).

The modal energy content of the POD mode m and the cumulative TKE fraction at modes $\leq m$ are illustrated in Figure 7. The modal energy content decays as $m^{-1/2}$, which is slower than the $m^{-0.9}$ decay as predicted by VerHulst & Meneveau (2014) for temporal snapshots 3 flow-through times apart. To complement the analysis, the modal content and the cumulative fraction for the vorticity based POD modes (maximizing turbulent enstrophy) are also illustrated in Figure 7. While around 25 velocity POD modes are required to capture 25% of the TKE, around 210 vorticity POD modes are necessary to capture around 25% of the turbulent enstrophy. This illustrates that enstrophy is more evenly distributed even at higher modes than the kinetic energy analogous to what we observe in the spectral picture of the turbulent kinetic energy and dissipation.

The dynamics of the POD modes can be better understood once the modes are projected onto the snapshots, which essentially generates the coefficients $a_m(t_n)$ of the POD basis expansion. The projections taken in the inner product sense yield $(u_i'(\mathbf{x},t_n)\,\phi_m^i(\mathbf{x}))_\Omega = a_m(t_n)$, considering the orthonormality of the POD bases $(\phi_k^i(\mathbf{x}),\phi_l^i(\mathbf{x}))_\Omega = \delta_{kl}$. The spectral picture in Figure 8 of the projection coefficients at different modes m reveal that the modal dynamics of the TKE manifest their maximum difference at lower frequency or larger time scales, while the projections of the vorticity modes manifest differences even at larger frequency scales. This further corroborates the idea that the dynamics of enstrophy (surrogate of dissipation) can be observed at smaller time scales as well, while it is mostly concentrated at relatively larger scales for the turbulent kinetic energy.

The modal pictures in Figures 9 and 10 reveal interesting flow structures for the flow past the wind turbines. Apart from the structures reminiscent of the roller-modes with counter rotating eddies with diameters $\gg D$ as observed in VerHulst & Meneveau (2014) (Refer to Figure 10 with $m=1,2,4,5$), the streamwise variation of the POD modes (Figure 9) also reveals large structures greater than the turbine rotor diameter inclined to the wall at $30^\circ - 60^\circ$. These inclined structures might be due to the inner layer growth and streamise inhomogeneity, or they might be a manifestation of the interaction of wind turbines with the near-wall dynamics. Interestingly, for the most energetic POD mode $m=1$, the roller mode structures also display "obtuse angle structures" in the top of the computational domain (Figure 9). Coupled with more detailed analysis, these structures also seem promising in understanding the localized dynamics of the vertical entrainment of the mean kinetic energy flux contributing to turbine power.

The roller-modes structures were known to have a significant contribution to the power generation in wind farms as predicted in VerHulst & Meneveau (2014). In infinite wind farms, the flux difference of the mean kinetic energy entrainment at the top and bottom rotor tip , i.e. $-\overline{u_i'u_j'}\bar{U}_i\Big|_{z_h-D/2}^{z_h+D/2}$ is known to be a significant contributor to power. In finite scale wind farms, due to the growth of the inner layer and wake impingements, the MKE flux is not the sole contributor to the farm power, but still plays a major role in the power generation. Table 1 shows the modal contribution of turbulent kinetic energy λ_m and the mean kinetic energy flux $-\lambda_m\phi_m^j\phi_m^j\overline{U}_i$ for the first 9 modes. This clearly indicates that a significant fraction of the MKE flux is captured by far less number of modes than turbulent kinetic energy, for which the POD modes are optimized in the least squares sense along the lines of VerHulst & Meneveau (2014). Table 1 further illustrates the significance of the roller modes ($m \leq 5$) as being instrumental to the MKE flux generation, the entrainment of which contributes to turbine power.

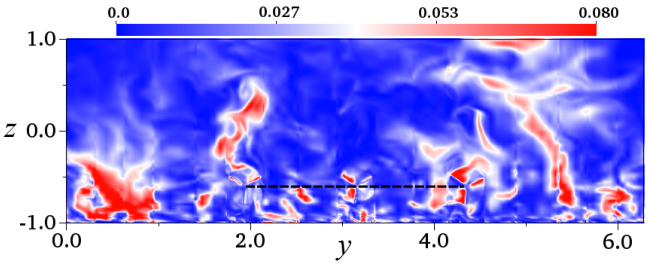

Figure 6: Snapshot of the yz plane (first row of turbines) of kinetic energy of the fluctuations normalized by free stream kinetic energy $\frac{1}{2}U_\infty^2$. Dashed black line connects the center of the rotor of the three turbines in the first row.

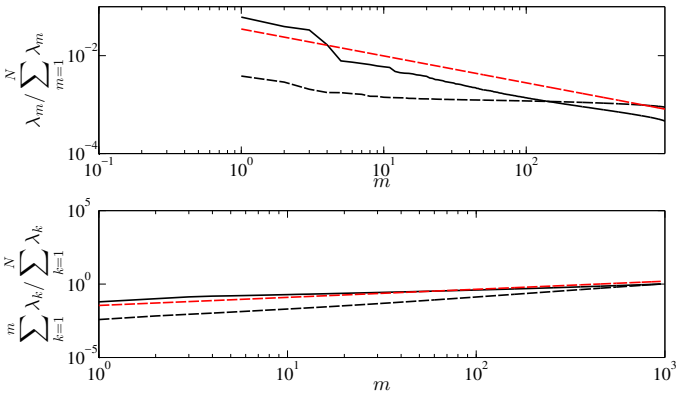

Figure 7: Top: Modal energy content (solid black), modal enstrophy content (dashed black) at each mode m. Red dashed – fitted $m^{-1/2}$ decay. Bottom: Cumulative modal energy content (solid black) and modal enstrophy content (dashed black) at each mode m. Red dashed – fitted $m^{1/2}$ growth

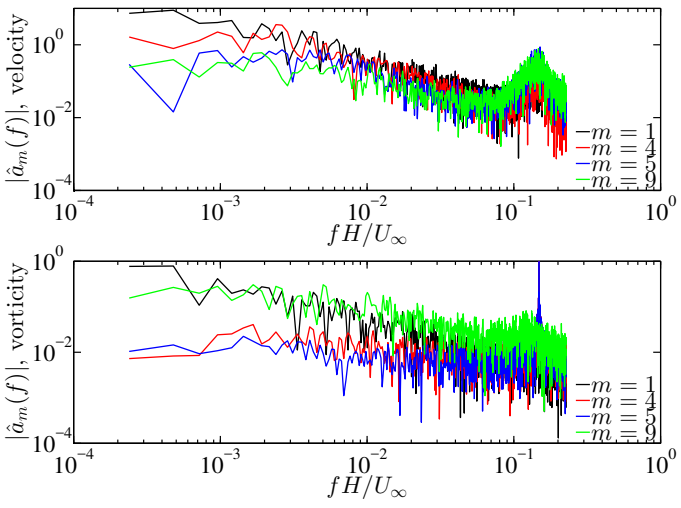

Figure 8: Top: Power spectral density of the projection of 4 velocity POD modes. Bottom: Power spectral density of the projection of 4 vorticity POD modes. $\hat{a}_m$ – Fourier transform of modal coefficient a_m

CONCLUSION AND FUTURE WORK

Existence of large scale flow features and their dynamics that contribute to the power in finite scale wind farms have been studied in the current paper. The finite scale wind farms manifest features of inhomogeneity in the streamwise direction that are not present in the periodic wind farm models in the asymptotic limit. Despite that, the modal pictures from the POD illustrate that structures reminiscent of large scale "roller-modes" with counter-rotating eddies as in VerHulst & Meneveau (2014) are observed in our simulations as well. However, because of the inhomogeneity in the flow (aperiodic domain and turbine location) the roller-mode structures do not appear quite as organized in the flow domain and streamwise variations are observed as well. Higher order modes have also displayed an "oblique structure phenomenon" inclined with the bottom "wall". Whether the acute angle structures are an interaction of the wind turbines with the near-wall dynamics and flow features, or whether these structures are generated due to the "growth of the inner layer" or streamwise inhomogeneity further needs to be explored in future. We also observed inclined structures at the free stream region (top of the computational domain) for $m = 1$ roller modes which have a significant contribution to the MKE flux entrainment and thus to the turbine power. These inclined structures show promise in understanding the localized dynamics of the MKE flux entrainment with streamwise growing inner layer that may contribute to power. As a final remark, even though in the current study only the MKE flux entrainment has been analyzed to understand the contribution to power, as a future work, we also plan to extend our study to understand the modal structure of the convective momentum and pressure gradient terms, which also contribute to the power generation in finite scale wind farms with streamwise inhomogeneity. These analysis would supposedly help us get a clearer picture of the behaviour of different length and time scales in the power generation of finite scale wind farms.

POD mode	Contribution to TKE (%)	Contribution to MKE flux difference (%)
1	6.13	12.88
2	3.93	4.05
3	3.34	3.31
4	1.67	2.76
5	0.78	1.18
6	0.74	0.88
7	0.69	0.68
8	0.66	0.57
9	0.62	0.54

Table 1: Contribution to turbulent kinetic energy $1/2\overline{u_i'u_i'}$ and mean kinetic energy flux difference $-\overline{u_i'u_j'}\bar{U}_i\Big|_{z_h-D/2}^{z_h+D/2}$ for the first 9 modes.

REFERENCES

Berkooz, G., Holmes, P. & Lumely, J. L. 1993 The proper orthogonal decomposition in the analysis of turbulent flows. *Annu. Rev. Fluid. Mech.* **25**, 539–575.

Bou-Zeid, E., Meneveau, C. & Parlange, M. 2005 A scale-dependant Lagrangian dynamic model for large eddy simulation of complex turbulent flows. *Phys. Fluids* **415**, 025125.

Calaf, M., Meneveau, C. & Meyers, J. 2010 Large eddy simulation study of fully developed wind-turbine array boundary layers. *Phys. Fluids* **22**, 015110.

Chatterjee, T. & Peet, Y. 2016*a* Large eddy simulation of a 3 × 3 wind turbine array using actuator line model with spectral elements. AIAA paper 2016–1988. 04 - 8 January 2016, San Diego, California.

Chatterjee, T. & Peet, Y. 2016*b* Spectra and large eddy structures

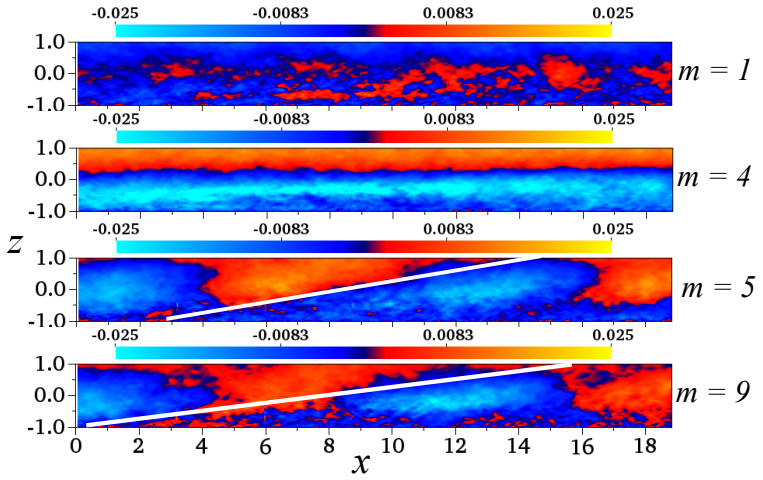

Figure 9: xz plane ($y = \pi H$) of the streamwise u POD modes $\phi_m^1\sqrt{\lambda_m}/U_\infty$ for 4 different modes maximizing turbulent kinetic energy $1/2\overline{u_i'u_i'}$.

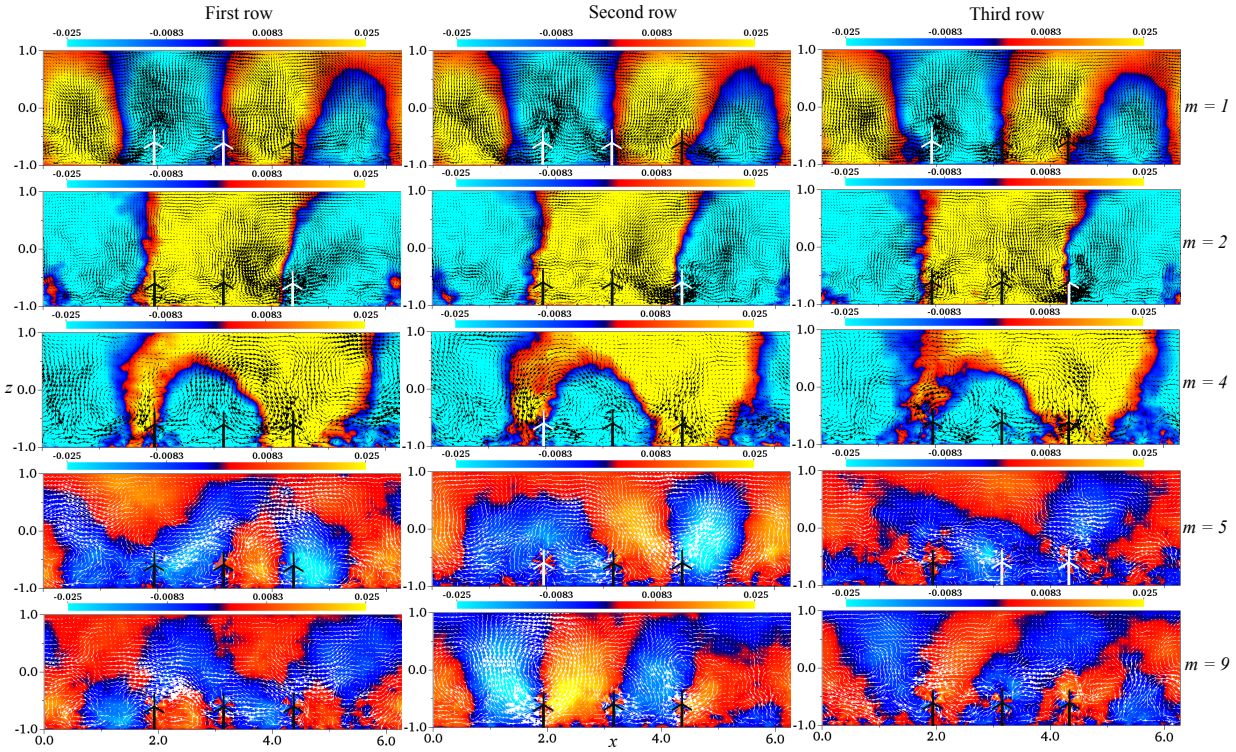

Figure 10: yz plane of the streamwise u POD modes $\phi_m^1\sqrt{\lambda_m}/U_\infty$ (contour) and spanwise, wall normal i.e., v, w POD modes $\phi_m^2\sqrt{\lambda_m}/U_\infty$, $\phi_m^3\sqrt{\lambda_m}/U_\infty$ (in-plane vectors) at 3 rows of turbines for 5 different modes, maximizing turbulent kinetic energy $1/2\overline{u_i'u_i'}$.

in the double log-layer in a high Re wind turbine array boundary layer. ASME Turbo Expo GT2016-56359.

Fischer, P., Lottes, J., Pointer, D. & Siegel, A. 2008 Petascale algorithms for reactor hydrodynamics. *J. Phys. Conf. Series* **125**, 012076.

Frandsen, S., ans S. Pryor, R. Barthelmie, Rathmann, O., Larsen, S., Hojstrup, J. & Thogersen, M. 2006 Analytical modelling of wind speed deficit in large offshore wind farms. *Wind Energy* **9**.

Hamilton, N., Tutkun, M., & Cal, R. B. 2016 Low-order representations of the canonical wind turbine array boundary layer via double proper orthogonal decomposition. *Phys. Fluids* **28**, 025103.

Merzari, Elia, Pointer, W. D. & Fischer, P. 2011 A pod-based solver for the advection-diffusion equation. Proceedings of ASME-JSME-KSME Joint Fluids Engineering Conference AJK2011–01022. July 24–29, 2011, Hamamatsu, Shizuoka, Japan.

Perry, A. E., Henbest, S. & Chong, M. S. 1986 Theoretical and experimental studies of wall turbulence. *J. Fluid. Mech.* **165**, 163–199.

Sirovich, L. 1987 Turbulence and the dynamics of coherent structures. part I: Coherent structures. *Q. J. Appl. Math.* **XLV**, 561–571.

VerHulst, C. & Meneveau, C. 2014 Large eddy simulation study of the kinetic energy entrainment by energetic turbulent flow structures in large wind farms. *Phys. Fluids* **26**, 025113.